JOURNAL OF MATERIALS SCIENCE 33 (1998) 4035–4041

Structural analysis of phases and heterophase interfaces in the zirconium–boron system

Y. CHAMPION*, S. HAGÈGE
CNRS-CECM, 15 rue G. Urbain, 94407 Vitry-sur-seine, France
E-mail: champion@glvt-cnrs.fr.

M. MASSE
ENSCP Laboratoire de Métallurgie Structurale, 11 Rue P. et M. Curie, 75231 Paris, France

The $\alpha Zr–ZrB_2$ eutectic, a model system for metal–boride interfaces, was prepared by r.f. induction melting from high-purity zirconium ingots and zirconium diboride powders. At the eutectic composition and depending on the cooling rate, the formation of either the ZrB phase or a Zr(B) solid solution has been observed in addition to the expected compound αZr and ZrB_2. For slow cooling rates, the formation of the compound ZrB by a peritectoid reaction and most likely stabilized by light elements (carbon, nitrogen, oxygen) has been observed. After rapid quenching, TEM investigations revealed the formation of a zirconium-based metastable phase; this new phase, with a nearly fcc structure, has been found in thin foils and is directly related to hexagonal αZr by a Shoji–Nishiyama orientation relationship. The structure at interfaces with habit planes featured by trigonal symmetry ($\{0\,0\,0\,1\}$ for hexagonal and $\{111\}$ for fcc), has been investigated using weak-beam diffraction contrast and high-resolution transmission electron microscopy. The interfaces with a small difference in lattice parameter are accommodated by a misfit dislocation network, whilst those with a large difference in lattice parameter exhibit a more complex structure with ledges and facets.

1. Introduction

Metal IVB–boride intermetallics $(Ti–Zr–Hf)B_2$ have attracted substantial interest on account of their extreme chemical and physical properties [1,2]. More specifically, they exhibit corrosion resistance, high electrical and thermal conductivity, high hardness and strength, thermal-shock and oxidation resistance at high temperature. By combination of these properties, borides should find technological applications for high-temperature devices in the aircraft and refractory industries. So far, they have been used as an alternative to oxide compounds in metal or alloy matrix composites [3]. The good wettability by molten aluminium has also promoted the fabrication of TiB_2 cathodes for electro-metallurgical industries [4, 5]. Moreover, coatings on titanium metallic devices subjected to high rate frictions has been emphasized recently as an alternative application for titanium or zirconium boride. However, one of the limiting factors for their most efficient use, is the fabrication of high-strength metal–metal boride interfaces for long-lasting coatings.

In the present study, this problem was primarily investigated through the analysis of the phases and heterophase interfaces which are likely to be produced in the Zr–B system. The Zr–B binary system has been selected as a model case study. According to the phase diagram, interfaces can be produced *in situ* from the high-temperature eutectic composition $\beta Zr–ZrB_2$ and subsequent solid phase transformations yield the formation of energetically favourable configurations for the interfaces. In addition, the formation of $\alpha Zr–ZrB_2$ is directly possible, while the isomorphic interface $\alpha Ti–TiB_2$ may not be directly obtainable for the production of the stable compounds TiB and Ti_3B_4 at room temperature.

This paper will essentially focus on the structure and composition of the phases and interfaces with dense habit planes, produced through the preparation procedure used, and subsequent thermal treatments. In a preliminary study [6], the existence of the zirconium monoboride compound was confirmed and most probably stabilized by impurities, mainly carbon, nitrogen and oxygen. Unlike the results mentioned in the literature [7–9], we have found that ZrB is easily stabilized at room temperature after slow cooling. In addition, a nearly f c c metastable form of zirconium, denoted χZr, has been identified in specimens obtained after fast cooling rate. A systematic experimental study of the orientation relationships between the phases which are likely to coexist in our samples was reported in a recent paper [10]: two main

* Author to whom all correspondence should be addressed.

types of orientation relationship between the compact phases (the hexagonal phases αZr ($P6_3/mmc$) and ZrB_2 ($P6/mmm$), the fcc phases χZr ($Fm\bar{3}m$) and ZrB ($Fm\bar{3}m$)) were found with the parallelism of the densest plane and directions of each structure. A group-theory analysis, accounting for the phase-transformation paths related to the thermal treatments and interface symmetries, stresses the fact that these experimentally observed configurations should be the most energetically favourable ones.

The preparations of the eutectic αZr–ZrB_2 compound and the thermal treatments are reported here, along with the phase structure and the phase transformations analysis. Interfaces with dense atomic habit plane have been analysed by weak-beam and high-resolution electron microscopy experiments and differences in interface structure have been related to the lattice misfit.

2. Preparation and phase analysis

Samples at the eutectic composition Zr–ZrB_2 (1.9 wt% boron) were prepared using r.f. induction (STEL generator, 500 kHz, 25 kW) and heated to about 2000°C to reach the melting point of zirconium and to dissolve the ZrB_2 powders in the molten liquid. After complete homogenization of the liquid, the mixture was cooled to 1680 °C for eutectic solidification to occur, producing ZrB_2 needles embedded in βZr single grains. In order to limit external contamination, the ingots were prepared in a water-cooled copper hearth, under a continuous high-purity argon flow. The zirconium used was prepared by the Van Arkel process and was therefore of very high purity; the ZrB_2 used was a commerical powder (99.5 wt% purity). Specimens for TEM were cut from the central part of the ingots, mechanically polished down to 50 μm thickness and then resized to a 3 mm disc. Thinning was completed by argon-ion beam milling. TEM foils were investigated using a 2000EX Jeol (200 kV) for conventional and weak-beam experiments. High-resolution electron microscopy (HREM) was carried out on an Akashi Topcon 002B (200 kV, $C_s = 0.4$ mm, point resolution = 0.18 nm). Fig. 1a shows the morphology of a ZrB_2 needle for a slowly cooled specimen (0.5 Ks^{-1}) and Fig. 1b that for a rapidly cooled specimen (100 Ks^{-1}). Needles are larger and interfaces flatter for slow cooling thermal treatment. For faster cooling rates, ledges are present at the interfaces and the needles are about ten times narrower.

Zirconium monoboride (ZrB) was observed in the samples obtained after slow cooling of specimens, and were identified with the NaCl type structure, by selected-area electron and X-ray diffraction. Portnoi and Romashov [9] proposed that the presence of impurities such as carbon, nitrogen and oxygen, is most likely a stabilizing factor in the formation of ZrB and is due partly to the high reactivity of Zirconium. Imaging by conventional electron microscopy reveals the phase to be present as an interlayer growing at the zirconium/zirconium diboride interface [6]. The lattice parameter of ZrB, measured by X-ray

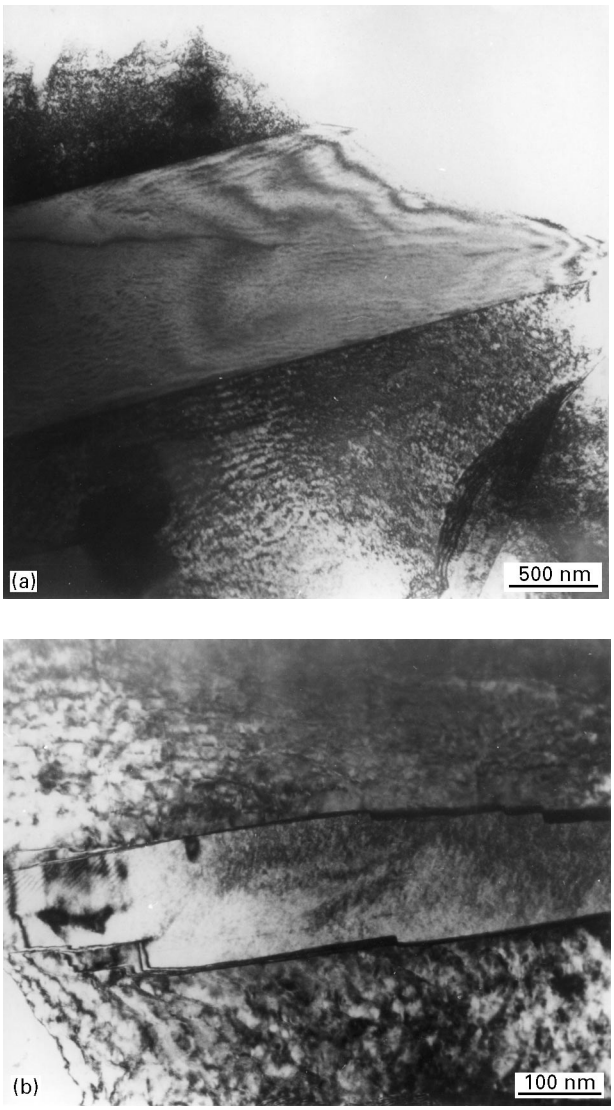

Figure 1 Transmission electron micrograph of a ZrB_2 needle embedded in an αZr matrix, (a) produced by growth during slow cooling; (b) produced by growth during fast cooling.

experiments, is 0.471 nm, and is consistent with the value proposed by Haggerty *et al.* [11] on ZrB precipitates produced by boron evaporation from ZrB_2 single crystal.

Owing to the presence of impurities and of the zirconium monoboride, the phase diagram proposed by Glaser and Post [7] was used instead of the current Zr–B phase diagram [12]. This work suggested that ZrB phase appears by a peritectoid reaction at 1250 °C between βZr and ZrB_2. As proof, after solidification, part of the samples were annealed at 1300 °C for 1h and then cooled relatively quickly to room temperature. ZrB was not found in these samples. This indicates that only the equilibrium between βZr and ZrB_2 phases is likely to coexist above this temperature and that the phase transformation for the formation of the monoboride is not allowed, because of slow atomic diffusion.

Further investigations on the same rapidly quenched specimens systematically revealed in thin areas of the TEM foils, an unusual close-fcc zirconium phase that the authors have denoted χZr. The phase boundary αZr–χZr, imaged along a common zone axes on

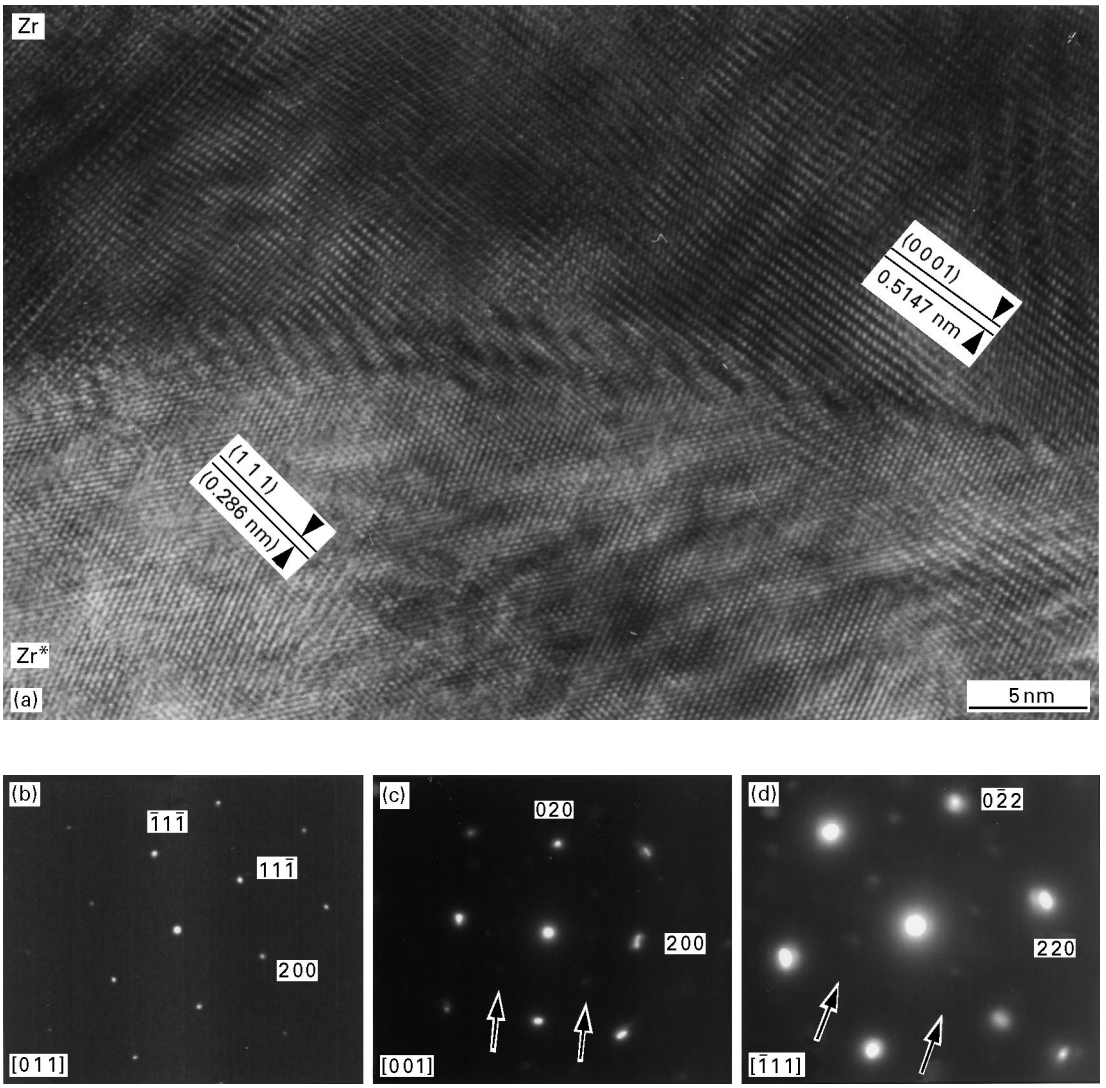

Figure 2 (a) HREM image of an αZr–χZr phase boundary in the [1 1 2 0] α‖[0 1 1]$_\chi$ projection. (b–d) Related patterns of the χZr related to a nearly fcc structure.

the HREM image (Fig. 2a), indicates directly that χZr is produced by a phase transformation of the α phase following the Shoji–Nishiyama orientation: [1 1 $\bar{2}$ 0] α‖[0 1 1]χ and (0 0 0 1) α‖(1 1 1)χ. Fig. 2b–d are electron diffraction patterns of the χZr phase. Careful measurements in the reciprocal space indicate that the structure is slightly elongated and/or sheared with respect to a face-centred cubic structure. Moreover, on the 0 0 1 zone axis of Fig. 3c, extra spots with a lower brightness are present at some of the positions of the fcc forbidden reflections 0 0 1 and 0 1 1. According to the indexing, only the 1 0 0 and $\bar{1}$ 0 0 reflections are missing from the pattern. The parameter of the approximate fcc structure of χZr, measured from those diffraction patterns is 0.496 nm. The deformation of the unit cell, such as elongation, compression or shear, cannot be responsible for the occurrence of extra reflections. These can only be due to a change in the lattice symmetry or, in other words, to a change in the chemical ordering of the unit cell.

According to the phase diagram, the stable form of zirconium at high temperature forms a solid solution with boron upto 1.5 at%. This concentration of boron can be retained at room temperature after fast cooling. However, boron is now not in equilibrium in a solid solution with αZr and this unstable configuration can yield the α–χ phase transformation. This new phase will have to be stabilized through a joint effect, combining the energy provided by the Ar^+ ion milling and a thin foil effect. The low impurity content found in χZr [13] cannot, by itself, account for the intensity present at the fcc forbidden reflection positions, as observed on the 0 0 1 zone axis. This effect will have to be ascribed to slight displacements of zirconium atoms with respect to the fcc Bravais cell.

3. Interface structure

The heterophases investigated are in the equivalent orientation relationships:

$$(0\,0\,0\,1) \parallel (0\,0\,0\,1) \text{ and } [1\,1\,\bar{2}\,0] \parallel [1\,1\,\bar{2}\,0]$$

$$(0\,0\,0\,1) \parallel (1\,1\,1) \text{ and } [1\,1\bar{2}\,0] \parallel [1\,1\,0]$$

As the (0 0 0 1) plane of the hexagonal structure and the (1 1 1) plane of the fcc structure have the same two-dimensional trigonal symmetry, a similar mode of accommodation at the interfaces with such a habit

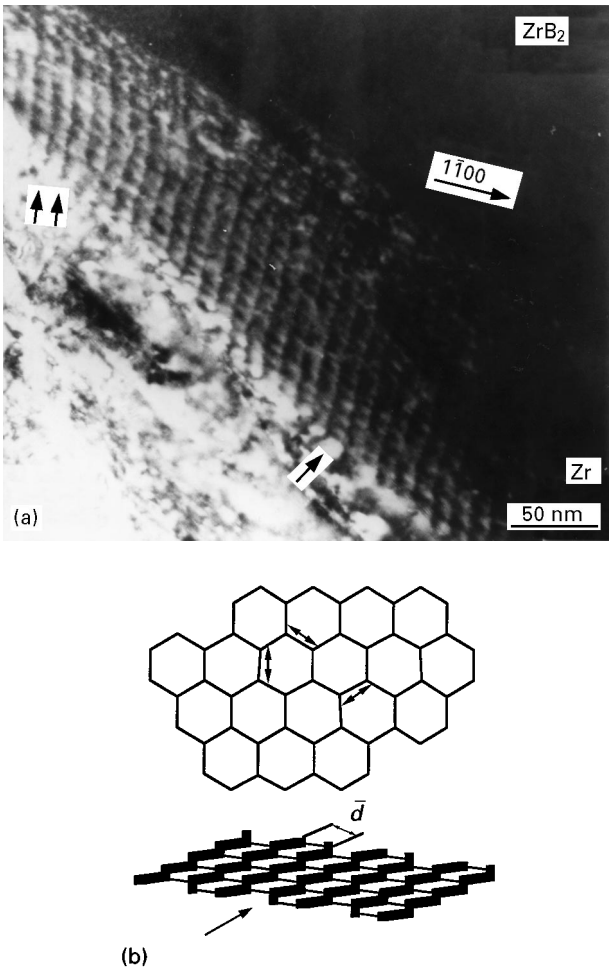

Figure 3 (a) TEM weak-beam image ($g = 1\bar{1}00$) of a (0001) αZr–ZrB_2 interface, revealing two sets of misfit dislocations (bright contrasts). (b) Schematic drawing of a hexagonal network in projection along a tilted direction. The thick lines composed of long and short segments depict the dislocation network observed in the weak-beam image.

plane should be expected, in as much as the lattice misfit is not too different. This is the case for the αZr–$ZrBr_2$, αZr–ZrB which are featured by a low misfit 2% and 3%, respectively. The structure at these interfaces may be compared with that at the χZr–ZrB_2, featuring a high 10% misfit.

Weak-beam experiments on an αZr–ZrB_2 interface reveal a set of periodic lattice strain contrasts related to misfit dislocations (Fig. 3). In this study, the weak-beam method, as well as "two-beam" bright-field conditions, were used only to observe the geometry of the dislocation network. The weak beam is a convenient method for imaging well-separated dislocations from their related lattice distortion. Moreover, the type of contrast produced by the weak beam allows us to distinguish between lattice distortion and Moiré fringes which are not obvious in bright-field conditions. This image is for a nearly two-beam condition using a reflection $g = 1\bar{1}00$ of the ZrB_2 phase, therefore implying that only a part of the total dislocation network is imaged. In fact, two sets of dislocation lines can be seen on this image even if one of them is drastically shortened by the projection. This effect is illustrated in the inset of Fig. 3 and demonstrates the wave-like structure of the weak-beam contrasts. The single arrow in the figure points to a slightly misoriented zone of the boundary revealing, in the dark-field condition the projected hexagonal dislocation network. The actual mean projected periodicity is

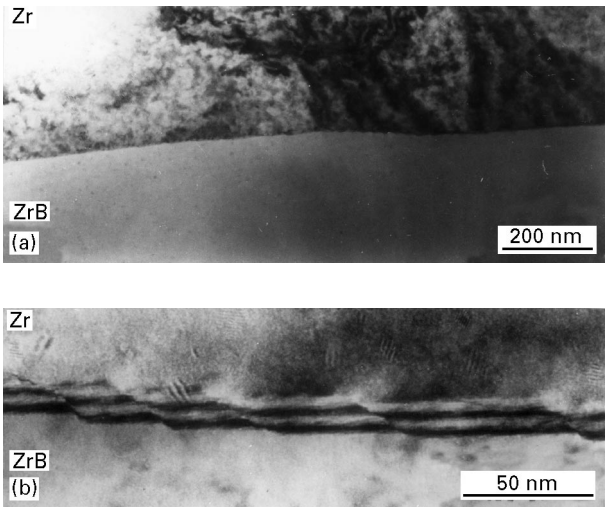

Figure 4 Bright-field TEM image of an αZr–ZrB interface exhibiting a curved boundary (a) which can be resolved as facets (b) at higher magnification.

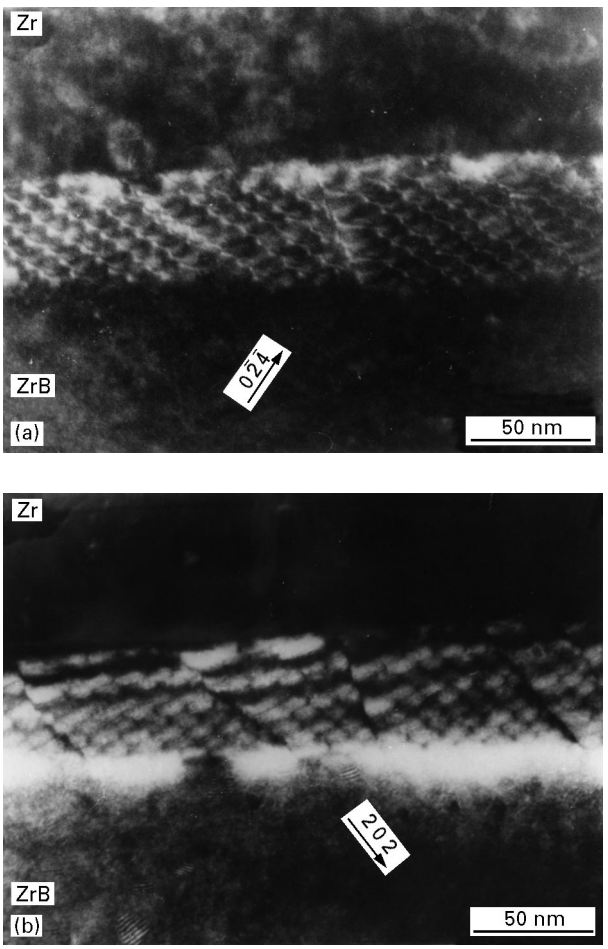

Figure 5 (a) TEM weak-beam image ($g = 0\bar{2}\bar{4}$) of an αZr–ZrB interface with two sets of misfit dislocations (bright contrasts) on the (0001), (111) facets. (b) Dark-field ($g = 202$) with the entire dislocation network (in dark contrast).

measured as $\bar{d} = 14$ nm, which corresponds to a dislocation interspacing of $d = 2\ \bar{d}/3^{1/2} = 162$ nm.

Similar weak-beam experiments were performed at a αZr–ZrB interface. Now, the interface is not flat at low magnification (Fig. 4a) and appears at larger magnification to be composed of a nanometre scale of (0 0 0 1)–(1 1 1) facets separated by ledges (Fig. 4b). The weak-beam image in Fig. 5a ($g = 0\,\bar{2}\,\bar{4}$) indicates the presence of misfit dislocations at the facet planes, very similar to the case of the αZr–ZrB_2 interfaces. This observation also corresponds to the situation depicted in Fig. 3. The hexagonal shape of the overall misfit dislocation network is revealed on the dark-field image performed with the reflection $g = 202$ (Fig. 5b). For this network, the dislocation interspacing measured is 12 nm and the direction of the lines is parallel to the common $\langle 1\,0\,\bar{1}\,0\rangle$, $\langle 2\,1\,1\rangle$.

The dislocation networks were modelled geometrically, using the misfit concept first introduced by Brooks [14]. The difference in lattice parameter along an interface is seen as a set of additional planes within the crystal having the smallest lattice distance, each additional plane being located between two successive areas of good matching. In order to minimize the interfacial energy, a network of dislocations has to be considered and their Burgers vector is directly related to the additional translation introduced by the difference in lattice parameter. The structure and geometry of the overall two-dimensional misfit dislocation network is governed by the symmetry of the planes in contact at the interface, the orientation relationship, and the misfit. A superposition of the atomic configuration in contact at the interface locates the good and bad matching zones at the interface (Fig. 6a) and consequently the misfit dislocation network (Fig. 6b). In these approaches, the dislocation lines are parallel to the $\langle 1\,0\,\bar{1}\,0\rangle$, $\langle 2\,1\,1\rangle$ direction in perfect agreement with the experimental result on the αZr–ZrB interface. The distance between dislocations lines (11 nm for αZr–ZrB and 16 nm for αZr–ZrB_2) is given by $d = a_1/\delta$, with a_1 the lattice I interspacing and δ the misfit parameter calculated from $\delta = 2|a_2 - a_1|/|a_2 + a_1|$, with a_2 the lattice II interspacing. For a hexagonal lattice, the interspacing a_i is the lattice parameter a, whereas for the fcc lattice, a_i is the modulus of the vector $a/2[1\,\bar{1}\,0]$ with a, the lattice parameter of the cubic structure. Despite the roughness of this analysis, the experimental results and

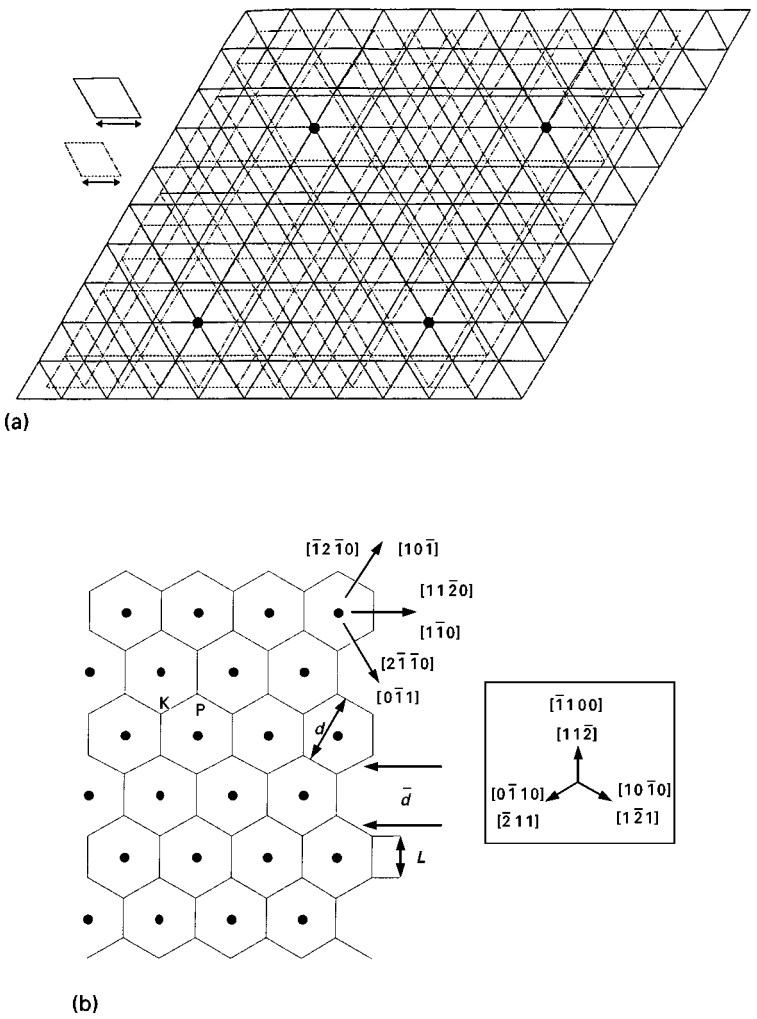

Figure 6 Superposition of two two-dimensional hexagonal networks depicting the αZr–ZrB_2 and αZr–ZrB interfaces). The parameter difference gives rise to a hexagonal net of good matching zones or coincident nodes (black dots) and bad matching zones. (b) The resulting misfit dislocation network is constructed by locating a dislocation segment inbetween two adjacent coincident nodes.

the modelling are fairly consistent for the interface $\alpha Zr–ZrB_2$, whilst for $\alpha Zr–ZrB$, an 8% difference arises between the dislocation distance measured and calculated. This discrepancy may be ascribed to the αZr lattice expansion at the interface, induced by ZrB having larger plane interspacings. Brooks [14] emphasized very early that the modelling should be calculated with the strained lattice parameters, but such values remain rather difficult to measure experimentally because the strain field is localized over few atomic planes parallel to the interface. For the case study, considering ZrB as infinitely rigid in comparison with the metal, the discrepancy would indicate a 0.25% swelling of the αZr lattice.

For the $\chi Zr–ZrB_2$ interface, no line contrast was observed in the bright field or by the weak method, and further investigation were done by high-resolution electron microscopy. Fig. 7 is a projection of the two structures along the common $[0\,\bar{1}\,1] \parallel [1\,1\,\bar{2}\,0]$ zone axes. Based on comparisons with image simulations, the thickness of the sample and the defocusing of the image were estimated to be respectively 10 nm and -50 nm with white contrasts on the zirconium columns for both χZr and ZrB_2. In the presence of zirconium ($Z = 40$) the boron atoms are not detectable on the simulated images and experimental contrasts can be directly connected to the two sublattices of zirconium. The variation of the image contrast reveals, from left to right, a long and flat interface along the $(1\,1\,1)\|(0\,0\,0\,1)$ habit plane, a high ledge with a $(2\,\bar{1}\,\bar{1}) \parallel [1\,\bar{1}\,0\,0]$ habit plane, and a somewhat more disordered interface which will not be taken into consideration hereafter.

Although the $\chi Zr–ZrB_2(1\,1\,1) \parallel (0\,0\,0\,1)$ interface has the same two-dimensional symmetry as the $\alpha Zr–ZrB_2$ and $\alpha Zr–ZrB$ interfaces, the mode of accommodation is definitely different. A careful examination of the boundary area (Fig. 7b), shows large zones of good matching, despite the 10% misfit. In any event, a hexagonal $a/3\langle 1\,1\,\bar{2}\,0\rangle$ dislocation network does not appear to be involved in the accommodation of the interface. If this had been the case, the dislocation lines would have been inclined with respect to the zone axis of the experimental HREM image. Then they would have exhibited an extended loss of resolution at the interface associated with a periodic arrangement of a poor matching zone, as observed by Lu and Cosandey [15] (this period would have been of about 10 $(1\,\bar{1}\,0\,0)$ interplanar spacing of ZrB_2, for 10% misfit at the interface). It is suggested, instead, that

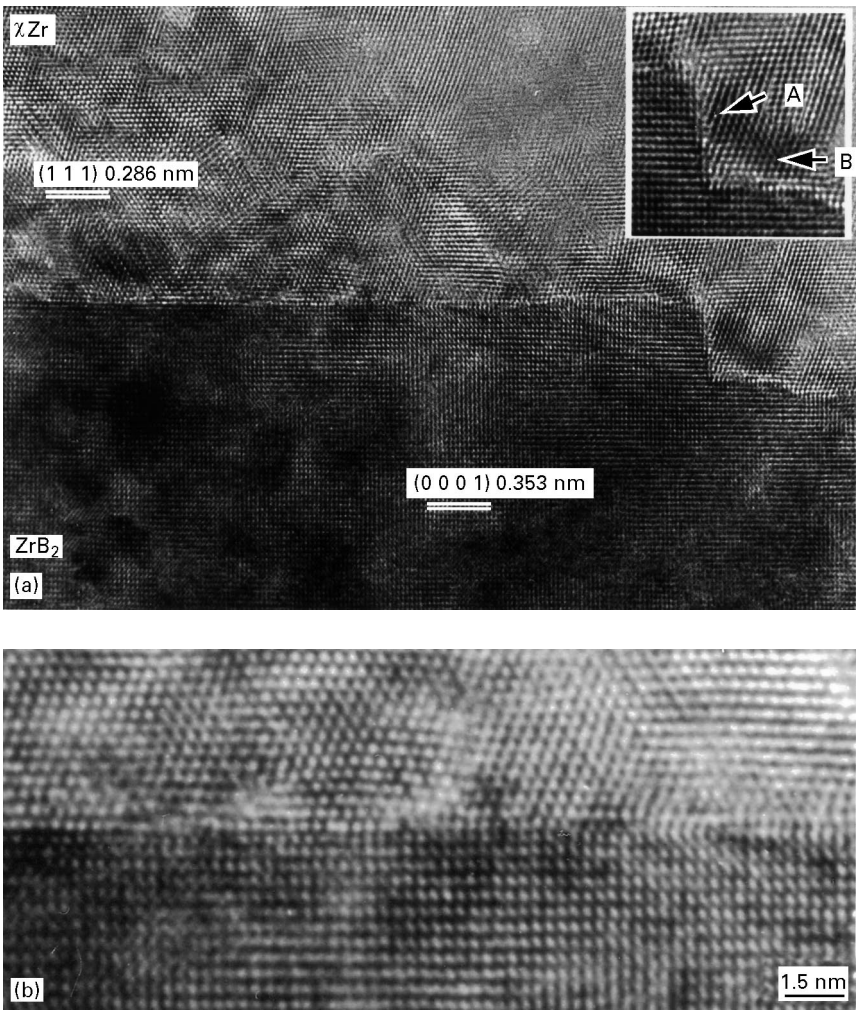

Figure 7 (a) HREM image of a type I $\chi Zr–ZrB_2$ interphase in the $[0\,\bar{1}\,1] \parallel [1\,1\,\bar{2}\,0]$ projection. White dots are related to the zirconium atomic columns in the two phases. Inset enlargement of the $[1\,\bar{1}\,0\,0] \parallel [2\,\bar{1}\,\bar{1}]$ $\chi Zr–ZrB_2$; arrows A and B indicate a monatomic step at the interface and a stand-off dislocation in χZr, respectively. (b) Higher magnification view of the interface area.

a misfit as large as 10% could be compensated by a set of monoatomic ledges, the structure and arrangement of which would depend on the lattices crystallographic structures, on their mutual orientation and on the lattices parameter misfit [16].

On considering the contact plane $(1\,\bar{1}\,0\,0)$, $(2\,\bar{1}\,\bar{1})$, the facet of the high ledge shown in the inset of Fig. 7a has to accommodate 21% misfit between the dense atomic planes perpendicular to the ledge; (0 0 0 1) for simple hexagonal in ZrB_2 and (1 1 1) for fcc in χZr. The experimental image reveals a monatomic step located in the middle of the ledge (arrow A), which is likely to be involved in such a structural matching in the boundary plane. The misfit appears to be compensated by a dislocation within the χZr lattice in the lower part of the ledge (arrow B) and by an 18% swelling of the χZr lattice in the [1 1 1] direction in the upper part.

4. Conclusion

In a preliminary stage, the present paper has reported an analysis of the composition and structure of heterophase interfaces produced for specific thermal conditions. The interphases were prepared *in situ* by eutectic solidification from a homogeneous high-temperature liquid mixture. Sample preparation combined r.f. induction in order to reach high temperature and subsequent thermal treatment, a copper hearth water-cool, and an inert atmosphere control limited the contamination.

Despite concern about the purity, it appeared that the ZrB phase is formed at the αZr–ZrB_2 interface and is stabilized at room temperature after a slow cooling, finally providing αZr–ZrB and ZrB–ZrB_2 interfaces. For rapid cooling, the formation of ZrB is impeded, but boron is likely to be retained at room temperature in a χZr(B) phase with a nearly fcc structure.

The interfaces present in our samples have been analysed by weak-beam and HREM. From these systems, always characterized by high symmetry orientation relationships, it arises that interfaces with a small misfit (about 3%) are accommodated by a network of dislocations. For a large misfit (about 10% or more), the accommodation is likely to be achieved by a complex arrangement of structural defects, which produce an apparent good matching at the interface as for the χZr–ZrB_2 (1 1 1) ∥ (0 0 0 1) interface.

Acknowledgements

This work was supported by the DGA/DRET under contract DRET/REP 93#93/1213. It is based, in part, on the thesis submitted by Y. Champion for the PhD degree in Materials Science, University Paris VI, France (1994). Van Arkel Zr was kindly provided by O. Dimitrov and J. Bigot (CECM- Vitry) and ZrB_2 powders were supplied by CERAC, Milwaukee, WI, USA.

References

1 I. M. LOW and R. McPHERSON, *J. mater. Sci. Lett.* **8** (1989) 1281.
2 H. ITOH, S. NAKA, T. MATSUDAIR and H. HAMAMOTO, *J. Mater. Sci.* **25** (1990) 533.
3 D. G. MORRIS and M. A. MORRIS, *Acta Metall. Mater.* **39** (1991) 1771.
4 H. R. BAUMGARTNER, *J. Am. Ceram. Soc.* **67** (1984) 490.
5 W. A. ZDANIEWSKI, *Am. Ceram. Bull.* **65** (1986) 1408.
6 Y. CHAMPION and S. HAGÈGE, *J. Mater. Sci. Lett.* **11** (1992) 290.
7 F. W. GLASER and B. POST, *Trans. Metall. Soc. AIME* **197** (1953) 1117.
8 K. I. PORTNOI, V. M. ROMASHOV and L. N. BUROBINA, *Sov. Powder Metall. Metal Ceram.* **91** (1970) 577.
9 K. I. PORTNOI and V. M. ROMASHOV, *ibid.* **113** (1972) 378.
10 Y. CHAMPION and S. HAGÈGE, *Acta Mater.* **44** (1996) 4169.
11 J. S. HAGGERTY, J. L. O'BRIEN and J. F. WENCKUS, *J. Crystal Growth* **3, 4** (1968) 291.
12 B. MASSALSKI, in "Binary alloys phase diagrams" (American Society for Metals, Metals Parks, OH, B. Massalski (ed.), 1990 p. 560.
13 Y. CHAMPION, M. MASSE, M. G. WALLS, M. TENCÉ and S. HAGÈGE, in "Proceedings of the Advanced Materials '93, III/B: Composites, Grain Boundaries and Nanophase Materials", edited by M. Sakai, Transactions of the Materials Research Society of Japan, Vol. 16B (Elsevier Science, Amsterdam, 1994) p. 1163.
14 H. BROOKS, in "Proceedings of 33rd Metal Congress" (ASM, Detroit, IL, 1951) p. 20.
15 P. LU and F. COSANDEY, *Ultramicroscopy* **40** (1992) 271.
16 Y. CHAMPION and S. HAGÈGE, *Interface Sci.* **4** (1997) 191.

Received 23 December 1997
and accepted 15 May 1998